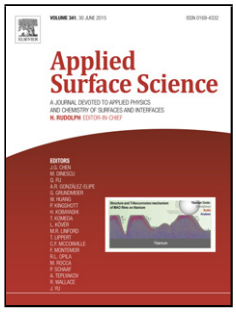

Title: Controlling the preferential orientation in sol-gel prepared $CaCu_3Ti_4O_{12}$ thin films by $LaAlO_3$ and $NdGaO_3$ substrates

Author: Suriyong Pongpaiboonkul Yumairah Kasa Ditsayut Phokharatkul Bundit Putasaeng Jose H. Hodak Anurat Wisitsoraat Satreerat K. Hodak

PII: S0169-4332(16)31120-5
DOI: http://dx.doi.org/doi:10.1016/j.apsusc.2016.05.101
Reference: APSUSC 33294

To appear in: *APSUSC*

Received date: 16-3-2016
Revised date: 15-5-2016
Accepted date: 19-5-2016

Please cite this article as: Suriyong Pongpaiboonkul, Yumairah Kasa, Ditsayut Phokharatkul, Bundit Putasaeng, Jose H.Hodak, Anurat Wisitsoraat, Satreerat K.Hodak, Controlling the preferential orientation in sol-gel prepared CaCu3Ti4O12 thin films by LaAlO3 and NdGaO3 substrates, Applied Surface Science http://dx.doi.org/10.1016/j.apsusc.2016.05.101

Controlling the preferential orientation in sol-gel prepared $CaCu_3Ti_4O_{12}$ thin films by $LaAlO_3$ and $NdGaO_3$ substrates

Suriyong Pongpaiboonkul[1], Yumairah Kasa[2], Ditsayut Phokharatkul[3], Bundit Putasaeng[4], Jose H. Hodak[2,5], Anurat Wisitsoraat[3], Satreerat K. Hodak[1,2*]

[1]Nanoscience and Nanotechnology Program, Center of Innovative Nanotechnology, Chulalongkorn University, Bangkok, 10330, Thailand

[2]Department of Physics, Faculty of Science, Chulalongkorn University, Bangkok, 10330, Thailand

[3]Nanoelectronics and MEMS laboratory, Pathumthani, 12120, Thailand

[4]National Metal and Materials Technology Center (MTEC), Thailand Science Park, Pathumthani 12120, Thailand

[5]DQIAyQF FCEN University of Buenos Aires/INQUIMAE-CONICET, Cdad,. Univ. Pab II, CABA, 1428, Buenos Aires, Argentina.

Corresponding author: satreerat.h@chula.ac.th, jeauw3@yahoo.com

Graphical Abstract

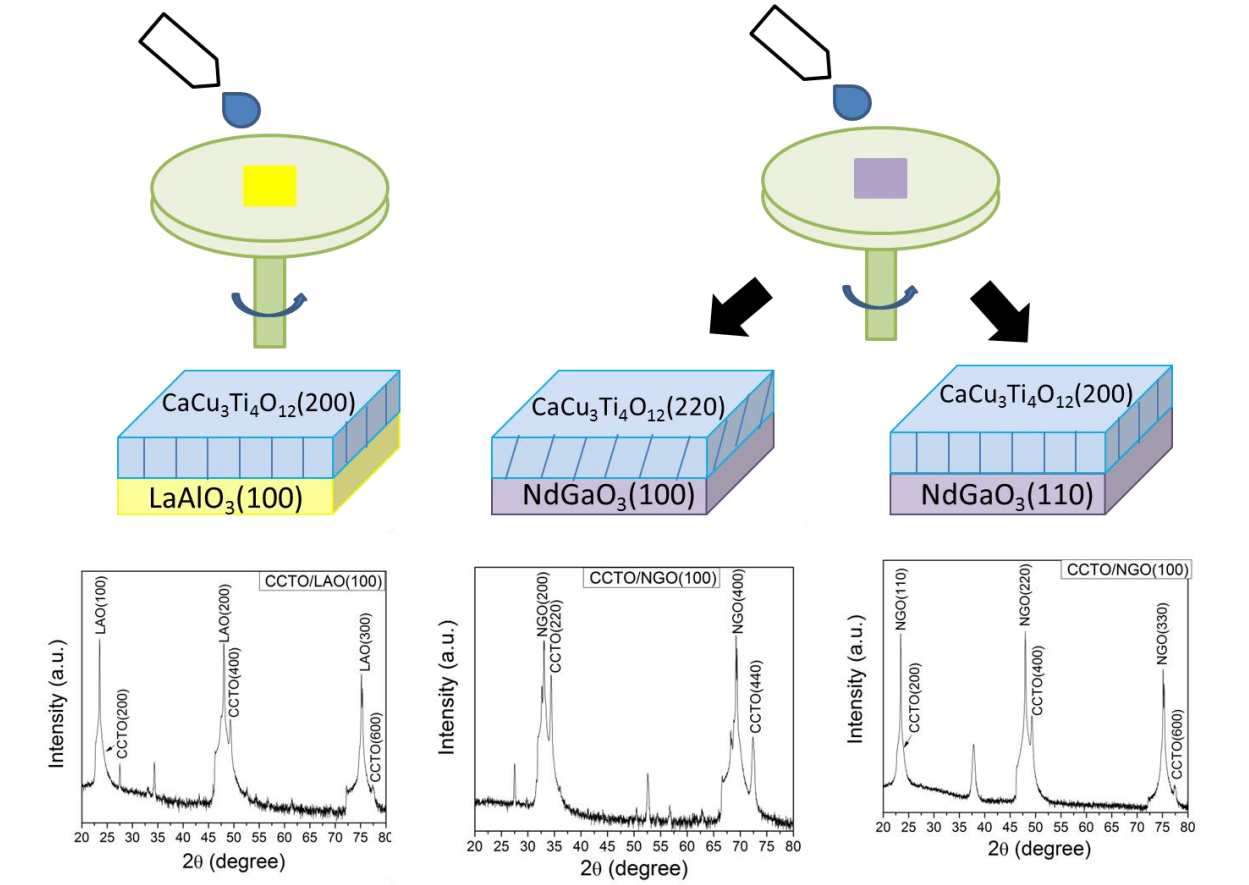

Highlights

- The preferred orientation of CCTO thin films can be manipulated to a high degree by growing it on specific crystal planes of the substrates without the use of buffer layers.

- X-ray diffraction signatures are the (*h*00) peaks for CCTO grown on both $LaAlO_3$(100) and $NdGaO_3$(110) substrates, and are the (*hh*0) peaks for the CCTO grown on $NdGaO_3$(100) substrate.

- The phase transition of the substrate affects the crystallinity of CCTO films and the alpha values for determining the degree of preferential orientation of the CCTO films; the optimum annealing temperature for CCTO on $LaAlO_3$ is 800 ºC and on $NdGaO_3$ is 1000 ºC.

- The grain size of CCTO films increases as the thickness and the annealing temperature increases.

- With the same annealing growth temperature of 1000 ºC, the CCTO/NGO(100) films yielded larger values of ε_r over the entire frequency range and loss tangents comparable with CCTO/LAO(100) at high frequency range.

Abstract

Researchers have paid considerable attention to $CaCu_3Ti_4O_{12}$ (CCTO) due to the colossal dielectric constant over a wide range of frequency and temperature. Despite of the growing number of works dealing with CCTO, there have been few studies of the role played by the substrate in inducing structural and dielectric effects of this material. In this work, highly-oriented CCTO thin films have been deposited on $LaAlO_3$(100), $NdGaO_3$(100) and $NdGaO_3$(110) substrates using a sol-gel method. These single crystal substrates were chosen in terms of small lattice mismatch between CCTO and the substrate. The X-ray diffraction patterns showed that the CCTO film layers grow with different orientations depending upon the substrate used. We show that the preferred orientation of CCTO thin films can be manipulated to a high degree by growing it on specific crystal planes of the substrates without the use of buffer layers. Colossal dielectric constants are observed in our films which appear to correlate with the film crystallinity and preferred orientation.

Keywords: Highly-oriented $CaCu_3Ti_4O_{12}$ films; $LaAlO_3$ substrate; $NdGaO_3$ substrate; Colossal dielectric constant and Sol-gel.

1. Introduction

Scaling of thin-film devices such as the integrated circuit capacitors for dynamic random access memory (DRAM) has been one of the most important issues in the microelectronic industry and related research fields. The vertical scaling of dielectric layer of capacitor is limited to a thickness of around 2 nm due to quantum mechanical tunneling effect so that the capacitance must alternatively be enhanced by increasing the dielectric constant. In recent years, $CaCu_3Ti_4O_{12}$ (CCTO) has been increasingly considered as the material of choice for nano-scale capacitive devices because of its colossal dielectric constant over wide temperature and frequency ranges of 100-600K and 1 kHz-1 MHz, respectively [1, 2]. One factor leading to this behavior is the lack of a ferroelectric transition in that temperature range. Unlike other ferroelectric or related dielectric materials such as (Ba, Sr)TiO_3 (BST) [3] and $SrTiO_3$ (STO) [4], ferroelectric lattice distortion have not been observed in CCTO by either high-resolution X-ray [5] or neutron powder diffraction experiments [1]. The dielectric constant of CCTO single crystal and ceramic are on the order of 10^5 and 10^4, respectively whereas that for the film form is in the range of 10^3-10^4 depending on whether the film is polycrystalline or epitaxial [6-8]. More importantly, the dielectric response of CCTO is strongly dependent on its microstructure and crystallinity. Several research groups have investigated the synthesis and characterization of CCTO thin films using different growth techniques including chemical and physical depositions. In the work of Prakash et al., the CCTO thin films were deposited on Pt/Ti/SiO_2/Si substrate using radio frequency magnetron sputtering and exhibited dielectric constants as high as 5000 at 400K at a frequency of 1 kHz [9]. Fang et al. have grown the CCTO thin films on Pt/Ti/SiO_2/Si

substrate using pulsed laser deposition which also exhibited fairly high dielectric constant, nearing 2000 at 10 kHz at room temperature [6]. Lin et al. have shown that the epitaxial CCTO thin films grown on $LaAlO_3$(001) by pulsed laser deposition reached even higher dielectric constants of ca. 10,000 at room temperature with a dielectric loss of 0.05 at 1 MHz [10]. High quality CCTO thin films could be epitaxially grown on various substrates with or without buffer or seed layers in order to increase the dielectric constant and suppress the dielectric loss [8]. CCTO films were grown on $LaNiO_3$ (LNO)-coated silicon substrates via a sol-gel method in which the conducting LNO acted as seed layer during the film growth [8]. Up to this date, there are only few reports on the influence of substrate types on the crystal structure and surface morphology of CCTO films and there are even fewer still dealing with sol-gel preparations [8, 11]. The CCTO films made by Li et al. exhibited (*h*00) preferential orientation on LNO-coated Si substrate [8]. The growth of CCTO films with (*h*00) preferential orientation on $SrTiO_3$ (100) (STO) substrates by using a chemical method have also been reported [11]. In selecting suitable substrates for CCTO growth, one has to consider that in the unit cell of the CCTO perovskite, there are eight TiO_6 octahedral sites tilted to form a square planar arrangement around Cu^{2+}[1, 12]. As a result of this, CCTO bulk ceramic has a cubic structure with a lattice constant of a =7.391 Å (space group *Im3*, $a^c = a/2$=3.696 Å) [1]. Furthermore, the choice of the crystal plane exposed by the substrate can have vastly different lattice constant relative to the CCTO footprint. Thus, substrates with perovskite structures cut along planes with lattice parameters matching the CCTO footprint are desirable. One such substrate, lanthanum aluminate ($LaAlO_3$, LAO), is a twinned rhombohedral structure at room temperature (space group $R\bar{3}m$) and undergoes a phase transition to a cubic structure (space group $Pm\bar{3}m$) at 813ºC [13]. The pseudo-cubic lattice parameter for LAO(100) is ca. 3.79 Å, resulting in a lattice mismatch of 2.5% between CCTO

film and the LAO substrate [14]. Neodymium gallate ($NdGaO_3$, NGO) single crystal substrate was found applicable to the growth of high-T_c superconducting thin films [15] and it was also suitable for deposition of perovskite dielectric thin films [16]. Because NGO has a distorted perovskite orthorhombic structure (space group *Pbnm*) and it does not undergo any phase transition until approximately 1300 ºC [13], it is a very promising substrate for achieving better epitaxial growth of CCTO thin films. The lattice parameters for NGO are $a = 5.44$ Å, $b = 5.50$ Å, and $c = 7.71$ Å, with corresponding pseudo-cubic lattice parameters of $a^c = 3.86$ Å and $b^c = c^c = 3.87$ Å (JCP Pattern No. 00-073-2299) [17]. Thus, the lattice mismatch between CCTO and pseudo-cubic NGO is about 4.4%. Furthermore, both LAO and NGO present the advantages of nearly matching the CCTO thermal expansion coefficient and have low dielectric constants. Compared with LAO, the main advantages of utilizing NGO as a substrate are the absence of twining effect and the lack of phase transitions in the temperature range of 800-1000 ºC needed for annealing CCTO. Therefore, NGO is an excellent candidate for fabricating hetero-interface highly-oriented CCTO perovskite structures. To the best of our knowledge there have been no studies of CCTO deposition on NGO. In this work, CCTO thin films were prepared on single crystal substrates of LAO(100), NGO(100) and NGO(110) by using a sol-gel method. The main goal of this work is to study the substrate inducing effects on the preferential orientation of the CCTO crystal phase in films made by a sol-gel method. The impacts of the substrate type on the crystal structure and the morphology of CCTO films are also explored. Our experimental results suggested that certain preferred orientations may have enhanced dielectric constant.

2. Experimental

2.1 Film synthesis

Films were deposited from sol-gel precursor solutions that we have previously optimized for deposition of mixed calchogenide titanates [18-20]. To prepare the film precursor solutions, 0.855 gram of calcium acetate hydrate ($Ca(C_2H_3O_2)_2 \cdot xH_2O$, Sigma-Aldrich, 99%) and 2.943 gram of copper (II) acetate monohydrate ($Cu(II)(C_2H_3O_2)_2 \cdot H_2O$, Fluka, 99%) were dissolved into glacial acetic acid (25 ml) and the solution was mixed by magnetic stirring for 24 hours at room temperature. After this period, the mixture was heated to 120 °C and a solution containing 6.12 gram of titanium (IV) isopropoxide ($Ti(OCH(CH_3)_2)_4$, Sigma-Aldrich, 97%), 3 ml of ethylene glycol ($C_2H_6O_2$, Sigma-Aldrich, 99%) and 3 ml of formamide ($HCONH_2$, Ranken, 99%) was added to it. The container was sealed and maintained at 120 °C for further 4-5 hours. The sol-gel precursor mixture was spin-coated on cleaned LAO and NGO substrates (size 1.0 cm×1.0 cm×0.05 cm) purchased from Surfacenet GmbH at a spin speed of 1500 rpm for 30 seconds. Each layer of the film was then baked on a hot plate at 120 ºC for 20 min and annealed in an oven with air atmosphere at 800 ºC and 1000ºC for 2 hours. During the annealing process, the temperature was ramped up with a rate of 5 ºC/min until it reached the desired temperature. After the annealing period, the temperature was ramped down with the same rate back to room temperature. Two and four cycles of spin coating were applied to each substrate to obtain different thickness of homogeneous, optically smooth and crack free films. The crystal structure of the films was analyzed using an X-Ray diffractometer (XRD:BRUKER model D8-Discover) equipped with a high-speed VANTEC detector and a Cu $K_{\alpha 1}$ X-ray source (λ = 0.15406 nm, 40 kV, 40 mA). The surface morphology, the cross section and the thickness of the films were investigated by field emission scanning electron microscopy (FE-SEM:HITACHI S-4700 Scanning Electron Microscope). The compositions of the films were analyzed by energy dispersive X-ray spectroscopy (EDS). Film coplanar capacitor devices were fabricated by

patterning aluminum/chromium (Al/Cr) interdigitated electrodes with 100 μm gap and 1500 μm finger length on the film by photolithography, sputtering and lift-off processes. [19, 21]. The dielectric constant and the corresponding loss tangent of our CCTO films were measured as a function of frequency at room temperature using a LCR analyzer (Model: 4294A, Agilent).

3. Results and discussion

3.1 Structural properties

Fig. 1 presents the XRD patterns of the CCTO films grown two (2L) and four (4L) layers on LAO(100) substrates annealed at 800 ºC and 1000 ºC, respectively. The intensity of the LAO substrate peaks is much stronger than that of CCTO films because the thickness of the substrate (~0.05 cm) is much larger than that for our films which is few hundreds of nanometers. Thus, to observe the film signals along with high diffraction peaks from the substrate, the intensities for the XRD patterns were plotted in log scale. This also allowed to best discriminate the secondary and impurity phases present in the films. The inset in Fig.1 shows a linear intensity scale representation of the same XRD pattern for the four-layered film annealed at 1000 ºC. Increasing the film thickness via depositing more layers also causes the peak intensities to increase. In polycrystalline CCTO films from other works, the dominant peaks are typically (220), (400), (422) and (440) [9, 12, 22]. Notably, in the case of our CCTO films for all the studied growth conditions, the (*h*00) were the most prominent reflections appearing at 2θ = 24.28º, 49.30º and 77.58º, and indexed as the (200), (400) and (600), respectively. Among the {*h00*} family, the

strongest peak is (400) while the (200) peak is overlapping with (100) diffraction peak from LAO substrate. Our XRD results are similar to those reported for CCTO grown by pulsed laser deposition on LAO(100) substrate [14]. Based on our analysis, using the strongest (400) peak position, our CCTO films have a cubic structure with estimated lattice parameters $a = b = c =$ 7.388 Å ($a^c = a/2 = 3.694$ Å), while LAO has a pseudo cubic structure with a calculated lattice constant of $a = 3.790$ Å.

It was concluded that our CCTO films deposited on LAO(100) substrates tend to be predominantly (*h*00) oriented. This indicates that the CCTO film layers grow with the *a*-axis perpendicular to the substrate surface. According to these findings, the in-plane alignment for CCTO is expected to be $[010]_{CCTO}$ // $[010]_{LAO}$ and $[001]_{CCTO}$ // $[001]_{LAO}$ [23]. The films also contain a small contribution of the CCTO(220) orientation. The intensity for the (220) peaks also increased as the film thickness increased from two-layered deposition to four-layered deposition. Small amounts of TiO_2 impurity phases were detected, consisting of only TiO_2 (004) anatase for films annealed at 800 ºC and only TiO_2 (110) rutile for films annealed at 1000 ºC. As seen in the inset in Fig. 1, both TiO_2 and CCTO(200) peak intensities are much smaller than that for CCTO(400). For CCTO powders and ceramics, the maximum intensity is known to be the (220) peak. Thus, to compare the degree of (*h*00) preferential orientation of our films, the maximum (400) intensity peak chosen as representative of all (*h*00) peaks was used to define the ratio of (400)-orientation $\alpha_{(400)}$ relative to (220) peak for CCTO/LAO(100) films [8].

$$\alpha_{(400)} = \frac{I_{(400)}^{film}/(I_{(220)}^{film} + I_{(400)}^{film})}{I_{(400)}^{powder}/(I_{(220)}^{powder} + I_{(400)}^{powder})}, \quad (1)$$

where $I_{(400)}^{film}$ and $I_{(220)}^{film}$ are the intensities of (400) peak and (220) peak of CCTO film, respectively, $I_{(400)}^{powder}$ and $I_{(220)}^{powder}$ are the relative intensities of (400) peak and (220) peak of CCTO powder (JCP Pattern No. 01-075-1149) from the XRD database, respectively. If the value of $\alpha_{(400)}$ is larger than 1, the films are considered to be (400) preferentially oriented [8]. Another way of comparing the extent of preferential orientation among a series of films could be made by comparing ratios of diffraction intensities for the X-ray diffraction peaks corresponding to the direction of maximum preferential orientation, relative to a peak from a secondary orientation. In our CCTO/LAO(100) films, we considered the ratios $I_{(400)}^{film} / I_{(220)}^{film}$. This ratio increases as the (*h*00) orientation becomes more abundant relative to the (*hh*0). Table 1 shows the results of both criteria applied to a series of CCTO films deposited on LAO(100).

For CCTO grown on LAO(100), the deposition of two layers produced films with a thickness of ca. 200 nm which upon annealing at temperatures of 800 ºC and 1000 ºC and yielded $\alpha_{(400)}$ of 3.36 and 3.04, respectively. In the case of four-layered films annealed at 1000 ºC, the calculated $\alpha_{(400)}$ increased to 3.19 mainly due to increasing film thickness compared to the two-layered film annealed at the same temperature. For four-layered CCTO/LAO(100) film annealed at 800 ºC, the maximum value for $\alpha_{(400)}$ of 3.41 was obtained. By way of comparison, all of our values of $\alpha_{(400)}$ are higher than 2.17 the best value reported for CCTO thin film grown on LNO-coated Si substrate [8]. As it is expected, the $I_{(400)}^{film} / I_{(220)}^{film}$ ratios track the $\alpha_{(400)}$ values, however, this ratio is advantageous in the sense that it is evaluated within the same X-ray diffractometer and does not rely on a reference powder diffraction pattern. It is important to stress that we can attain

such high degree of preferred orientation without the use of a buffer layer which greatly simplifies the film fabrication. More interestingly, for the films of the same thickness annealed at 800 ºC the value of $\alpha_{(400)}$ were always larger than those corresponding to the films annealed at 1000 ºC. This is likely due to the phase transition from rhombohedral to cubic in the LAO substrate which is known to occur at 813 ºC [24] partially disrupting the preferential orientation achieved up to 800 ºC. Thus, for this case as the annealing temperature increases from 800 ºC to 1000 ºC, the intensity of the diffraction peaks decreases. To rationalize the origin of the preferential orientation, we compared the footprint of the CCTO unit cell with the atomic surface layout on LAO(100) plane. Fig. 2 (a-b) shows the diagrams of top views for the CCTO(200) plane and for the LAO(100) plane, respectively. The Cu, Ca and O atoms on the CCTO(200) plane form an array with square symmetry approximately 3.694 Å on each side whereas the surface arrangement on LAO(100) forms an array with square symmetry of approximately 3.790 Å.

The lattice mismatch was evaluated by taking the difference of in-plane lattice parameters between the film and the substrate, relative to the in-plane lattice parameter of the substrate, specifically, $\left|\frac{(3.694-3.790)}{3.790}\right| \times 100\% = 2.5\%$. This value is considered to be a rather small mismatch. The strain caused by this mismatch could be released by forming mild dislocations at the boundary with the substrate. As the film thickness increases beyond the critical thickness (h_c) the strain may gradually relax across the film, thus it is expected that thicker films will have stronger diffraction peaks and better defined preferred orientation, which is consistent with our observations.

We now wish to turn our attention to the CCTO grown on single crystal NGO substrates. Fig. 3 shows the XRD patterns of the CCTO films grown with different number of layers on NGO(100) substrates annealed at 800 °C and 1000 °C. In Fig. 3, the dominant X-ray diffraction signatures are the (*hh*0) peaks consisting of (220) and (440) CCTO reflections which are located next to the NGO(200) and (400) substrate peaks, respectively. This is in striking contrast with the films deposited on LAO(100) which induced a completely different CCTO orientation. In the case of films grown on NGO(100), the CCTO(441) peak was also detected, suggesting the presence of small amount of crystals with another orientation. This minority orientation is also in contrast with that found in films grown for the LAO(100) case where there was a small contribution of the CCTO(220) orientation. Another interesting result is that the intensities of the dominant peaks in CCTO/NGO(100), namely the (220) and (440), not only increase with the number of

layers but also with increasing the annealing temperature from 800 °C and 1000 °C. These results suggest an improvement in the degree of structural order at higher annealing temperatures. As the annealing temperature increases, the intensity of diffraction peaks increases due to better film crystallinity which is consistent with bigger grains seen in the FE-SEM image results. This is in agreement with our expectation, since the NGO substrate has its phase transition at 1300 °C [13], and it again contrasts with the films annealed on LAO(100) substrates. Fig. 3 also shows the presence of small signals of TiO_2 (110) rutile phase in the case of CCTO annealed at 1000 ºC as well as CuO(110) and (220) corresponding to a tenorite crystal structure (JPN number 00-048-1548) found at both 800 ºC and 1000 ºC annealing temperatures.

We used the same rationale as before to interpret the preferential orientation of the CCTO on NGO(100). From the X-ray patterns in Fig. 3, the highest (220) peak was used to calculate the lattice constant of CCTO film on NGO(100) substrate which assuming a cubic lattice, yielded $a = 7.372$ Å ($a/2 = 3.686$ Å). Fig. 4 (a-b) shows the in-plane view of CCTO(220) plane and the surface lattice for NGO(100), respectively. It can be seen that the Cu, Ca and Ti atoms in the surface layer of CCTO(220) form an array with rectangular symmetry with a short side of 3.686 Å and a long side of 5.214 Å. Meanwhile, the surface layer of NGO(100) also form a rectangular array with short and long sides of 3.855 Å and 5.50 Å, respectively. Our first expectation is that the CCTO film would adopt an in-plane atomic layout such that it matches that for the surface lattice of NGO(100). In the CCTO y-axis direction, the lattice mismatch is given by $\left|\frac{(3.686-3.855)}{3.855}\right| \times 100\% = 4.4\%$ whereas in the x-axis direction the lattice mismatch is larger, $\left|\frac{(5.214-5.50)}{5.50}\right| \times 100\% = 5.2\%$. In any case, these results represent a mismatch twice as large as in the case of CCTO/LAO(100). Nevertheless the rectangular symmetry of the atomic arrangement

on NGO(100) dictates that a rectangular footprint for the CCTO overlay would result in an areal mismatch which may be defined as $\varepsilon_{xy} = \left| \frac{d_x^{CCTO} d_y^{CCTO} - d_x^{NGO} d_y^{NGO}}{d_x^{NGO} d_y^{NGO}} \right| \times 100\% = 9.3\%$.

As a consequence of this, the (*h*00) orientation is suppressed, with the films adopting the (*hh*0) orientation. A large lattice mismatch between CCTO and NGO(100) could lead to sufficiently high strain energy that could be prevent the full epitaxial growth of CCTO, and tend to produce polycrystalline films. For sake of comparison, the work of Feng et al., showed that highly-oriented CCTO films grown on the $SrTiO_3$ (STO) substrates were actually polycrystalline due to the large lattice mismatch between CCTO and STO(100) (5.7%) [11]. In general, nearly complete relaxation of the mismatch strain occurs over a critical film thickness. This critical thickness decreases with increasing lattice mismatch. For our films the mismatch is larger for CCTO/NGO(100) than for CCTO/LAO(100). Thus, for films with the same total thickness, CCTO/NGO(100) films are expected to have a relaxed crystal structure over a larger fraction of the total film thickness, leading to more intense diffraction peaks compared to CCTO/LAO(100) films. It is worth to note that the formalism of Li et. al. [8] expressed by Eq. (1), cannot be applied in the analysis of preferential orientation of the CCTO/NGO(100) films, using the relative intensity of (220) peak compared to that of (400) or the (411) peaks. This occurs because the (400) and (411) reflections are almost completely suppressed by the strong preferential orientation adopted by CCTO on NGO(100) and are negligible with respect to the much stronger (220) reflection in the reference powder diffraction pattern of CCTO. Thus, instead of using the alpha values following reference [6], we adopt the ratio $I_{(220)}^{film} / I_{(411)}^{film}$ when comparing among our CCTO/NGO(100) film series (Table 2).

In the case of CCTO/NGO(100) films, the highest preferred orientation values were obtained in the four-layered CCTO/NGO(100) films annealed at 1000 °C. In contrast with the LAO substrate case, NGO does not undergo a phase transition during the annealing cycle, thus, the preferred orientation of the CCTO films is not disturbed. To validate the rationale employed in explaining the CCTO orientations found on LAO(100) and NGO(100), we deposited CCTO on an NGO(110) substrate. The CCTO film was deposited with four layers and it was annealed at 800 °C. As it is revealed by the X-ray diffraction pattern shown in Fig. 5 for CCTO deposited on the (110) facet of NGO, the film adopts the same preferred orientation as on LAO(100).

In Fig. 5, the strong peaks originated from the {*h*00} family of planes; (200), (400) and (600). The peak corresponding to the (200) plane could not be clearly observed due to the overlapping with the strong (110) diffraction peak from NGO. The X-ray diffraction pattern of the CCTO/NGO(110) is consistent with a rather high degree of (*h*00) preferred orientation.

Fig. 6 (a-b) is a side by side comparison of the in-plane views for CCTO(200) and for the pseudo-cubic NGO(110) crystal structure, respectively. The square footprint for CCTO matches the atomic layout for the (110) facet of the pseudo-cubic NGO lattice. While NGO has a pseudo-cubic lattice constant of 3.868 Å the calculated lattice constant for CCTO/NGO(110) is 7.387 Å ($a/2 = 3.693$ Å) The lattice parameters are indeed similar leading to an in-plane mismatch of 4.5% in the x and y directions. The obtained $\alpha_{(400)}$ for the 4L CCTO/NGO(110) film annealed at 800 ºC is 3.44 which is comparable to that obtained for CCTO/LAO(100) annealed at the same temperature. It may be concluded that our selected single crystal substrates offer potential advantage when it comes to controlling the preferred orientation for CCTO. For comparison the main characteristic peaks of the CCTO film deposited on Si(100) substrate are (220), (400), (422) and (440) [9, 12, 22] which indicate a weak preferential orientation in their polycrystalline films. We wish to note that the films contain small amounts of TiO_2 phases. Notably, there is no detectable TiO_2 rutile phase in the CCTO/NGO(100) films annealed at 800 ºC but only at 1000 ºC. This is consistent with the results from the CCTO/LAO(100) films annealed at the same temperatures (vide supra, Figs. 1 and 3). Decomposition of CCTO into oxides is not known to occur at these temperatures. In our case, slight imbalances in the composition of the sol-gel precursor solution from the exact CCTO stoichiometry are the most likely culprit for occurrence of these impurities. During the handling of the sol-gel precursor solution, exposure to moisture from the air causes some hydrolysis of the titanium alkoxide. As a result of this, a colloidal dispersion of TiO_2 nanoparticles is produced [25], which appear as an impurity in the films. In some cases, broad and weak anatase peaks are observed at low annealing temperatures while sharp peaks rutile tends to be more clearly observed at high annealing temperatures. Dispersed amorphous nanoparticles TiO_2 could produce broad and weak peaks or no diffraction signals at

all if the particle size is too small. As the film is annealed at high temperature and the CCTO crystals grow larger, the TiO_2 phase segregates into the voids between crystals. With the anatase-rutile phase transition at temperatures ranging between 730 ºC and 1200 ºC [26], recrystallization of the TiO_2 into more stable rutile may occur at these accumulation sites, which could explain why more intense diffraction peaks for rutile phase are more likely to be observed after annealing at 1000 ºC than at 800 ºC. The peaks for the impurity phases Signals due to CuO impurity have only been observed in the films on NGO(100), appearing at 32.51º and 68.12º and were respectively assigned to (110) and (220) of the tenorite structure [27]. As crude guideline for the abundance of impurities we note that the peak amplitudes for their diffraction peaks are much smaller than those for the CCTO phase. Although these films were cast from the exact same sol-gel precursor solution as the films deposited on LAO(100) and NGO(110), the CuO diffraction signals only occurred on films deposited on NGO(100). The reason for the specific appearance of CuO diffraction signatures on this particular substrate is not clear to us. One possible explanation is that CuO is present in dispersed form in all our films but sufficiently large crystals only grow on NGO(100) due the close match between the lattice spacing of tenorite and NGO(100). Experimental evidence supporting this is the CuO peaks appearing in close proximity with the (200) and (400) diffraction peaks of the (100) NGO substrates. The calculated d-lattice spacing for CuO(110) plane was 2.75 Å which is very close to the d-lattice spacing for NGO(200) plane (2.71 Å). The d-spacing for CuO(100) plane matches the Cu-Cu distance in the plane where Cu atoms are surrounded by four coplanar oxygen ions (Cu-O plane) [28]. Previous works have also directed attention to CuO phase as being present around the CCTO grain boundaries [27, 29, 30]. In those works, CuO was readily observed, especially in the films annealed at temperatures of 1000 °C and higher. In our films, the EDX experiments did not

confirm that the grain boundary regions are richer in Cu than the regions within the CCTO grains, which agrees with the results of other sol-gel prepared CCTO [31]. Whether the appearance of these copper rich grain boundaries depends on the film preparation method is still an unresolved issue and further research in this field is needed to completely understand the grain and boundary compositions in CCTO. Some other works often reported the appearance of impurity phases in their CCTO films. TiO_2 rutile phase was detected in sol-gel deposited films [31, 32], powders [7] and ceramics [33]. $CaTiO_3$ have also appeared in CCTO deposited on LAO using metal organic chemical vapor deposition (MOCVD) [34]. It appears to be that among all the deposition methods, pulsed laser deposition (PLD) under high temperature and high oxygen pressure may yield the highest purity CCTO films [6, 10, 35]. We wish to stress that our findings about the inducing effects of the substrate facet on the preferred orientation should also be applicable to higher purity films on LAO and NGO because they inherent to CCTO lattice parameters and to their relationship to those of the substrates.

3.2 Morphology properties

The influence of the substrate type on the preferential orientation of CCTO also has a strong impact on the grain size and morphology of the films. These effects were investigated using FE-SEM. Fig. 7 shows the films created by depositing two layers of CCTO on the (100) plane of LAO and NGO. Fig. 7(a-d) shows the films annealed at 800 °C, while Fig. 7(e-h) corresponds to films annealed at 1000 °C. The surface morphology of the films is shown on the left panels. Magnified surface images are shown on the right panels together with the cross-sectional view of the films. The grains for the films annealed at 1000 ºC are clearly larger than those for films annealed at 800 ºC, with slightly larger grains for CCTO/NGO(100) than for CCTO/LAO(100).

These results are consistent with our XRD data which shows more intense diffraction peaks for the films annealed at higher temperatures.

For all the films in Fig. 7, the surface morphologies are similar to those observed in the in other works [31]. The surface is crack-free but it presents a high degree of porosity, and a grain size which is not uniformly distributed over the films which appears to be a characteristic of the sol-gel prepared multilayer films [31]. Crudely speaking, we distinguish two types of morphology areas with different average grain sizes, which are labeled as areas (1) and (2) on the left panels of Fig. 7. The corresponding high magnification FE-SEM photographs in Fig.7 (b) and (d) for area (1), show that on LAO(100) and NGO(100) the CCTO annealed at 800 ºC have similar average grain sizes in the 40-60 nm range while for area (2) it is in 100-200 nm range. The cross section FE-SEM images clearly show that most of the voids and pores in the film do not pass all the way across to the interface with the substrate. The films annealed at 1000 ºC were more compact and less porous than those annealed at 800 ºC. The origin of these pores could be related to solvent evaporation during the preheating gas evolution due to pyrolysis of the acetate and isopropoxide species occurring during the treatment at higher temperatures [31]. At the annealing temperature of 1000 ºC, the thermal energy causes coalescence of the smaller clusters into larger crystals, and as a result of this process some of the porous structure of the films disappears. From Fig. 7(e-h) in area (2), the grain sizes for CCTO/LAO film are clearly smaller than that for CCTO/NGO film.

Fig. 8 shows the surface morphology of four-layered CCTO films deposited on the (100) plane of LAO and NGO. Fig. 8(a-d) shows the films annealed at 800 °C, while Fig. 8(e-h) depicts the films annealed at 1000 °C. The surface morphology of the films is shown on the left panels with magnified surface images shown in the insets. The cross-sectional view of the films is shown on

the right photographs of Fig. 8. Again larger grains are observed at higher annealing temperatures but the largest grains are obtained on NGO substrates. We have noticed that the porous structure is seen more often when the annealing time is too short and the temperature is too low. In our case, the porosity is much smaller for the films annealed at 1000 °C compared to the film annealed at 800 °C. The porosity also decreases in the thicker films obtained by deposition of additional CCTO layers. We observed that a considerable densification occurs during longer annealing at high temperatures which is consistent with a higher atomic mobility. An important feature of our work is that for films annealed at 1000 ºC the CCTO grain size is always larger on NGO than on LAO substrates, while for films annealed at 800 ºC the films contain similar grain size on either substrate. This is in line with our XRD observations and based on our previous analysis, we expect a more perfect annealing effect in NGO(100) than in LAO(100) which undergoes a phase transition in the annealing process. The interface between the CCTO film and NGO(100) shows a very sharp interface which implies negligible interdiffusion across the interface. In the case of the CCTO films deposited on NGO(110) facet, we observed grain sizes that are comparable to those for CCTO/NGO(100) and CCTO/LAO(100) films. Fig. 9 shows FE-SEM images of a four-layered CCTO film annealed at 800 ºC.

As expected, the thickness and morphological characteristics for the film shown on Fig. 9 (a-b), respectively are similar to the ones already discussed in Figs. 7 and 8, however, as it was shown in Fig. 5, the preferred orientation is totally different to that for the CCTO on LAO(100) and NGO(100). Depending on the desired applications for the films the choice of annealing temperature could be used to tailor the morphology and film porosity. For instance, in gas sensing application the lower annealing temperature produces higher porosity and thus, larger

surface area accessible to gas-film chemical interactions [19, 21]. In capacitor fabrication, the more dense films with larger grain sizes would be preferable for higher dielectric constant [16].

3.3 Dielectric properties

For characterizing the dielectric properties of the films, we selected the four-layered films because CCTO films with a thickness of less than 300 nm typically showed relative low dielectric constants nearing 700 [6, 14]. The studied CCTO films were grown to the same thickness of approximately 500 nm. The CCTO films on LAO(100) annealed at 800 ºC have considerably more imperfections than those annealed at 1000 ºC, despite of the fact that the preferential orientation (see $\alpha_{(400)}$ values in Table 1) on this substrate was slightly better when the annealing temperature lower than the phase transition temperature of LAO. For CCTO films grown on NGO(100) the best film characteristics in terms of surface morphology, crystallinity, namely denser films with lower porosity and larger crystal domain sizes, are obtained by annealing at 1000 ºC. Therefore we choose to compare the dielectric constant for films deposited on LAO(100) and NGO(100) and annealed at 1000 ºC. Dielectric measurements were carried out at room temperature in the frequency range from 1 kHz to 1 MHz. We fabricated capacitors by patterning a pair of interdigitated electrodes [21]. The capacitance data was analyzed according to the model derived by Fernell et al. [36]. Fig. 10(a-d) compares the dielectric constant and loss tangent results for our CCTO films grown on LAO(100) and NGO(100). Giant dielectric constant (ε_r) is observed for both of these films which is explained by the grain-boundary mechanism [2]. The occurrence of such high ε_r has been attributed to the electrically heterogeneous nature of the materials consisting of semiconducting grains surrounded by insulating grain boundaries, and it follows the relation [37]

$$\varepsilon_r = \varepsilon_{gb} \frac{t_g + t_{gb}}{t_{gb}} \quad (2)$$

where ε_{gb} is the dielectric constant of the grain boundary layer, t_g and t_{gb} are the thickness of the grain and grain boundary layers, respectively. At room temperature, dielectric constant of the CCTO thin films is much lower (~1700 at 10 kHz for CCTO/LAO and ~3800 at 10 kHz for CCTO/NGO) than that for bulk CCTO (~10^4). As the frequency increases, the dielectric constant first decreases drastically and then it approaches a constant value in the 10^6 to 10^7 Hz range. In contrast to what is commonly observed for CCTO bulk, there is a significant dielectric relaxation in our films measured in this frequency range, especially at low frequency range. It is known that oxygen vacancies and space charges (electrons) may be produced in the grain boundaries according to

O_O (Oxygen ion at its normal site) $\rightarrow$ V_O (Oxygen vacancy) $+ 2e^- + \frac{1}{2}O_2$, which could result in dielectric relaxation in the low frequency regime [35].

Consistent with other works, the giant dielectric constants in the CCTO films are accompanied by high values of dielectric losses. The dielectric loss has its origin in the resistive behavior of the free carriers and on dipole relaxation [38]. In the case of our films, due to the possible presence of oxygen vacancies and free electrons, the resistive loss could be the dominant mechanism.

In comparison, our results of dielectric constant and loss tangent for CCTO/LAO are close to those of Fang et al. ($\varepsilon_r \approx 2000$, $\tan\delta \approx 0.5$ @10 kHz) [6] for CCTO thin films prepared by pulsed-laser deposition on Pt/Ti/SiO_2/Si(100) substrates and to those of Singh et al. ($\varepsilon_r \approx 1500$, $\tan\delta \approx 0.15$ @10 kHz) by a sol-gel method deposition on Pt/Ti/SiO_2/Si(100) substrates

[39]. Notably, the CCTO/NGO(100) films yielded larger values of ε_r over the entire frequency range and loss tangents comparable with CCTO/LAO(100) at high frequency range. However, considering the entire frequency range in Fig. 10, the dielectric constant and loss tangent for CCTO/NGO(100) were 2.3 and 1.7 times higher, respectively than those corresponding to CCTO/LAO(100). Thus, there is a clear advantage in selecting the CCTO/NGO combination. This could be due to the larger grains but it might also be related to anisotropic values of ε_r and $\tan\delta$ yielding better parameters for (*hh*0) oriented CCTO than for (*h*00) oriented CCTO.

4. Conclusions

Highly-oriented $CaCu_3Ti_4O_{12}$ (CCTO) thin films were successfully deposited directly on LAO(100), NGO(100) and NGO(110) substrates using a sol-gel spinning method. Beside the similarity in lattice mismatch and the similarity in crystal structure between the film and the substrate, the orientation of the substrate is a crucial parameter for preferred orientation growth. We showed that the preferred orientation for the CCTO can be controlled by means of the selection the material and crystal plane used as substrate. Our experiments showed that the best single crystal substrate to obtain the highest dielectric constant for (*hh*0) preferential oriented CCTO film is NGO(100) while optimum growth of the (*h*00) oriented CCTO is possible on LAO(100), as well as on NGO(110). We found evidence suggesting that the occurrence of a phase transition in the LAO substrates is detrimental to the film quality. Thus, the optimum temperature for annealing CCTO films on LAO substrate is 800 ºC while for NGO substrates the annealing could be done at 1000 ºC. The dielectric constant was clearly larger in the film with larger grains. Our results suggest that better values of ε_r with comparatively low $\tan\delta$ result when the films acquire (*hh*0) orientation rather the (*h*00) orientation.

Acknowledgments

Authors would like to thank Center of Innovative Nanotechnology (CIN) and The 90th Anniversary of Chulalongkorn University Fund to support budgets for this research. This research has been supported by the Ratchadapiseksomphot Endowment Fund of Chulalongkorn University (RES560530227-AM). Jose H. Hodak thanks Chulalongkorn University for visiting professor fund, MINCYT for fund PICT-2041-2012 and University of Buenos Aires for the

UBACYT grant. We would like to specially thank to Dr. Adisorn Tuantranont and National Electronics and Computer Technology (NECTEC) for lithography facilities.

References

[1] M.A. Subramanian, D. Li, N. Duan, B.A. Reisner, A.W. Sleight, High dielectric constant in $ACu_3Ti_4O_{12}$ and $ACu_3Ti_3FeO_{12}$ phases, J. Solid State Chem., 151 (2000) 323-325.
[2] D.C. Sinclair, T.B. Adams, F.D. Morrison, A.R. West, $CaCu_3Ti_4O_{12}$: One-step internal barrier layer capacitor, Appl. Phys. Lett., 80 (2002) 2153-2155.
[3] D.E. Kotecki, J.D. Baniecki, H. Shen, R.B. Laibowitz, K.L. Saenger, J.J. Lian, T.M. Shaw, S.D. Athavale, C. Cabral, P.R. Duncombe, M. Gutsche, G. Kunkel, Y.J. Park, Y.Y. Wang, R. Wise, $(Ba,Sr)TiO_3$ dielectrics for future stacked- capacitor DRAM, IBM Journal of Research and Development, 43 (1999) 367-382.
[4] H.-C. Li, W. Si, A.D. West, X.X. Xi, Thickness dependence of dielectric loss in $SrTiO_3$ thin films, Appl. Phys. Lett., 73 (1998) 464-466.
[5] A.P. Ramirez, M.A. Subramanian, M. Gardel, G. Blumberg, D. Li, T. Vogt, S.M. Shapiro, Giant dielectric constant response in a copper-titanate, Solid State Commun., 115 (2000) 217-220.
[6] L. Fang, M. Shen, Deposition and dielectric properties of $CaCu_3Ti_4O_{12}$ thin films on $Pt/Ti/SiO_2/Si$ substrates using pulsed-laser deposition, Thin Solid Films, 440 (2003) 60-65.
[7] L. Liu, H. Fan, P. Fang, L. Jin, Electrical heterogeneity in $CaCu_3Ti_4O_{12}$ ceramics fabricated by sol–gel method, Solid State Commun., 142 (2007) 573-576.
[8] Y.W. Li, Z.G. Hu, J.L. Sun, X.J. Meng, J.H. Chu, Preparation and properties of $CaCu_3Ti_4O_{12}$ thin film grown on $LaNiO_3$-coated silicon by sol–gel process, J. Cryst. Growth, 310 (2008) 378-381.
[9] B.S. Prakash, K.B.R. Varma, D. Michau, M. Maglione, Deposition and dielectric properties of $CaCu_3Ti_4O_{12}$ thin films deposited on $Pt/Ti/SiO_2/Si$ substrates using radio frequency magnetron sputtering, Thin Solid Films, 516 (2008) 2874-2880.
[10] Y. Lin, Y.B. Chen, T. Garret, S.W. Liu, C.L. Chen, L. Chen, R.P. Bontchev, A. Jacobson, J.C. Jiang, E.I. Meletis, J. Horwitz, H.-D. Wu, Epitaxial growth of dielectric $CaCu_3Ti_4O_{12}$ thin films on (001) $LaAlO_3$ by pulsed laser deposition, Appl. Phys. Lett., 81 (2002) 631-633.
[11] L. Feng, Y. Wang, Y. Yan, G. Cao, Z. Jiao, Growth of highly-oriented $CaCu_3Ti_4O_{12}$ thin films on $SrTiO_3$ (1 0 0) substrates by a chemical solution route, Appl. Surf. Sci., 253 (2006) 2268-2271.
[12] M.A. Ramirez, A.Z. Simões, A.A. Felix, R. Tararam, E. Longo, J.A. Varela, Electric and dielectric behavior of $CaCu_3Ti_4O_{12}$-based thin films obtained by soft chemical method, J. Alloys Compd., 509 (2011) 9930-9933.
[13] L. Vasylechko, A. Senyshyn, U. Bismayer, Chapter 242 Perovskite-Type Aluminates and Gallates, in: Handbook on the Physics and Chemistry of Rare Earths, Elsevier, 2009, pp. 113-295.
[14] W. Si, E.M. Cruz, P.D. Johnson, P.W. Barnes, P. Woodward, A.P. Ramirez, Epitaxial thin films of the giant-dielectric-constant material $CaCu_3Ti_4O_{12}$ grown by pulsed-laser deposition, Appl. Phys. Lett., 81 (2002) 2056-2058.
[15] G. Koren, A. Gupta, E.A. Giess, A. Segmüller, R.B. Laibowitz, Epitaxial films of $YBa_2Cu_3O_{7-\delta}$ on $NdGaO_3$, $LaGaO_3$, and $SrTiO_3$ substrates deposited by laser ablation, Appl. Phys. Lett., 54 (1989) 1054-1056.

[16] S.K. Hodak, C.T. Rogers, Microstructure and dielectric response of $SrTiO_3/NdGaO_3$ interdigitated capacitors, Microelectron. Eng., 85 (2008) 444-451.
[17] D.L. Proffit, H.W. Jang, S. Lee, C.T. Nelson, X.Q. Pan, M.S. Rzchowski, C.B. Eom, Influence of symmetry mismatch on heteroepitaxial growth of perovskite thin films, Appl. Phys. Lett., 93 (2008) 111912.
[18] O. Kongwut, A. Kornduangkeaw, N. Jangsawang, S.K. Hodak, Influence of gamma irradiation on the refractive index of Fe-doped barium titanate thin films, Thin Solid Films, 518 (2010) 7407-7411.
[19] S. Pongpaiboonkul, D. Phokharatkul, J.H. Hodak, A. Wisitsoraat, S.K. Hodak, Enhancement of H_2S-sensing performances with Fe-doping in $CaCu_3Ti_4O_{12}$ thin films prepared by a sol–gel method, Sens. Actuators, A, 224 (2016) 118-127.
[20] T. Supasai, S. Dangtip, P. Learngarunsri, N. Boonyopakorn, A. Wisitsoraat, S.K. Hodak, Influence of temperature annealing on optical properties of $SrTiO_3/BaTiO_3$ multilayered films on indium tin oxide, Appl. Surf. Sci., 256 (2010) 4462-4467.
[21] S.K. Hodak, T. Supasai, A. Wisitsoraat, J.H. Hodak, Design of Low Cost Gas Sensor Based on $SrTiO_3$ and $BaTiO_3$ Films, Journal of Nanoscience and Nanotechnology, 10 (2010) 7236-7238.
[22] F. Moura, E.C. Aguiar, E. Longo, J.A. Varela, A.Z. Simões, Dielectric properties of soft chemical method derived $CaCu_3Ti_4O_{12}$ thin films onto $Pt/TiO_2/Si(1\ 0\ 0)$ substrates, J. Alloys Compd., 509 (2011) 3817-3821.
[23] J.C. Jiang †, E.I. Meletis, C.L. Chen, Y. Lin, Z. Zhang, W.K. Chu, Nanocomposite-like structure in an epitaxial $CaCu_3Ti_4O_{12}$ film on LaAlO3 (001), Philos. Mag. Lett., 84 (2004) 443-450.
[24] G.W. Berkstresser, A.J. Valentino, C.D. Brandle, Growth of single crystals of lanthanum aluminate, J. Cryst. Growth, 109 (1991) 457-466.
[25] K. Farhadian Azizi, M.-M. Bagheri-Mohagheghi, Transition from anatase to rutile phase in titanium dioxide (TiO_2) nanoparticles synthesized by complexing sol–gel process: effect of kind of complexing agent and calcinating temperature, J. Sol-Gel Sci. Technol., 65 (2012) 329-335.
[26] D.A.H. Hanaor, C.C. Sorrell, Review of the anatase to rutile phase transformation, Journal of Materials Science, 46 (2010) 855-874.
[27] J.J. Mohamed, S.D. Hutagalung, Z.A. Ahmad, Influence of sintering parameters on melting CuO phase in $CaCu_3Ti_4O_{12}$, Journal of King Saud University - Engineering Sciences, 25 (2013) 35-39.
[28] R. Kita, T. Hase, M. Sasaki, T. Morishita, S. Tanaka, Epitaxial growth of CuO thin films by in situ oxidation of Cu thin films, J. Cryst. Growth, 115 (1991) 752-757.
[29] L. Ni, X.M. Chen, X.Q. Liu, R.Z. Hou, Microstructure-dependent giant dielectric response in $CaCu_3Ti_4O_{12}$ ceramics, Solid State Commun., 139 (2006) 45-50.
[30] T. Li, Z. Chen, Y. Su, L. Su, J. Zhang, Effect of grain size and Cu-rich phase on the electric properties of $CaCu_3Ti_4O_{12}$ ceramics, Journal of Materials Science, 44 (2009) 6149-6154.
[31] D. Xu, K. He, R. Yu, X. Sun, Y. Yang, H. Xu, H. Yuan, J. Ma, High dielectric permittivity and low dielectric loss in sol–gel derived Zn doped $CaCu_3Ti_4O_{12}$ thin films, Mater. Chem. Phys., 153 (2015) 229-235.
[32] R. Parra, E. Joanni, J.W.M. Espinosa, R. Tararam, M. Cilense, P.R. Bueno, J.A. Varela, E. Longo, Photoluminescent $CaCu_3Ti_4O_{12}$-Based Thin Films Synthesized by a Sol–Gel Method, J. Am. Ceram. Soc., 91 (2008) 4162-4164.

[33] X. Ouyang, M. Habib, P. Cao, S. Wei, Z. Huang, W. Zhang, W. Gao, Enhanced extrinsic dielectric response of TiO_2 modified $CaCu_3Ti_4O_{12}$ ceramics, Ceram. Int., 41 (2015) 13447-13454.
[34] R.L. Nigro, R.G. Toro, G. Malandrino, I.L. Fragalà, P. Fiorenza, V. Raineri, Effects of high temperature annealing on MOCVD grown $CaCu_3Ti_4O_{12}$ films on $LaAlO_3$ substrates, Surf. Coat. Technol., 201 (2007) 9243-9247.
[35] L. Fang, M. Shen, W. Cao, Effects of postanneal conditions on the dielectric properties of $CaCu_3Ti_4O_{12}$ thin films prepared on Pt/Ti/SiO_2/Si substrates, J. Appl. Phys., 95 (2004) 6483-6485.
[36] G.W. Farnell, I.A. Cermak, P. Silverster, S.K. Wong, Capacitance and Field Distributions for Interdigital Surface-Wave Transducers, Sonics and Ultrasonics, IEEE Transactions on, 17 (1970) 188-195.
[37] L. Singh, U.S. Rai, K.D. Mandal, N.B. Singh, Progress in the growth of $CaCu_3Ti_4O_{12}$ and related functional dielectric perovskites, Prog. Cryst. Growth Charact. Mater., 60 (2014) 15-62.
[38] L. Fang, M. Shen, J. Yang, Z. Li, Reduced dielectric loss and leakage current in $CaCu_3Ti_4O_{12}$/SiO_2/$CaCu_3Ti_4O_{12}$ multilayered films, Solid State Commun., 137 (2006) 381-386.
[39] D.P. Singh, Y.N. Mohapatra, D.C. Agrawal, Dielectric and leakage current properties of sol–gel derived calcium copper titanate (CCTO) thin films and CCTO/ZrO_2 multilayers, Mater. Sci. Eng., B, 157 (2009) 58-65.

Figure Captions

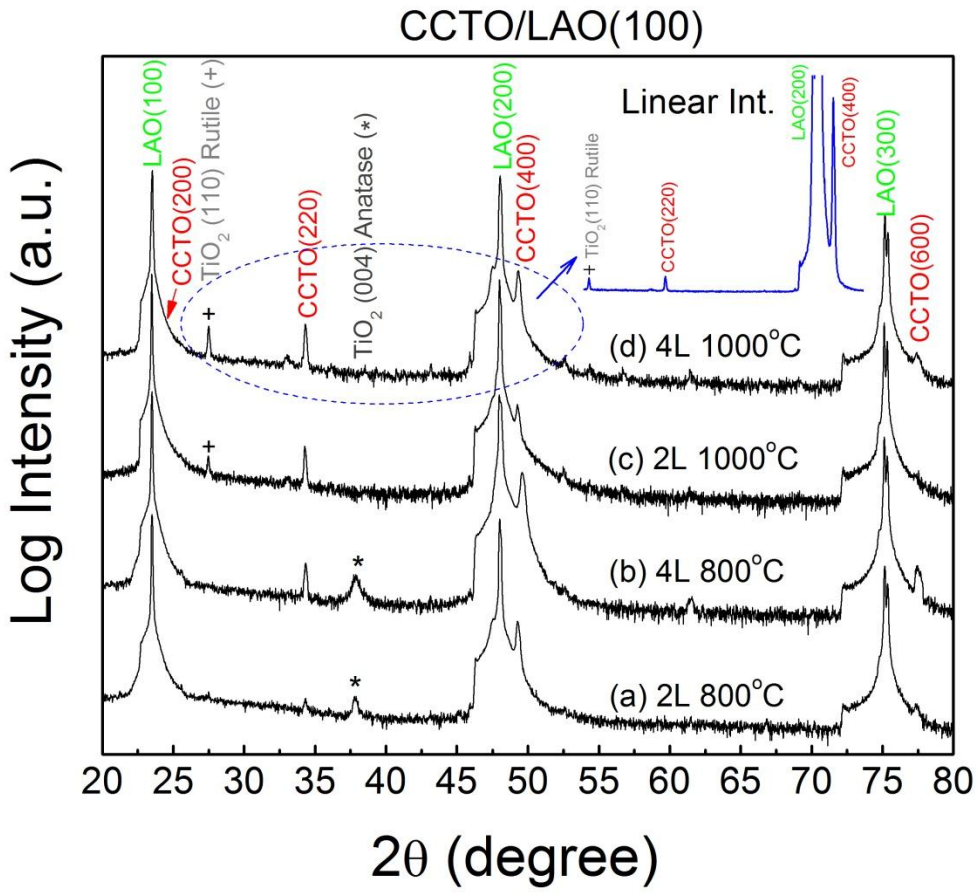

Fig. 1 θ-2θ X-ray diffraction scans of CCTO films deposited on LAO (100) substrates: (a) two-layered CCTO/LAO(100) annealed at 800 ºC, (b) four-layered CCTO/LAO(100) annealed at 800 ºC, (c) two-layered CCTO/LAO(100) annealed at 1000 ºC, (d) four-layered CCTO/LAO(100) annealed at 1000 ºC. Note that the main plot is in log scale while the inset is the XRD pattern in linear intensity scale for film (d).

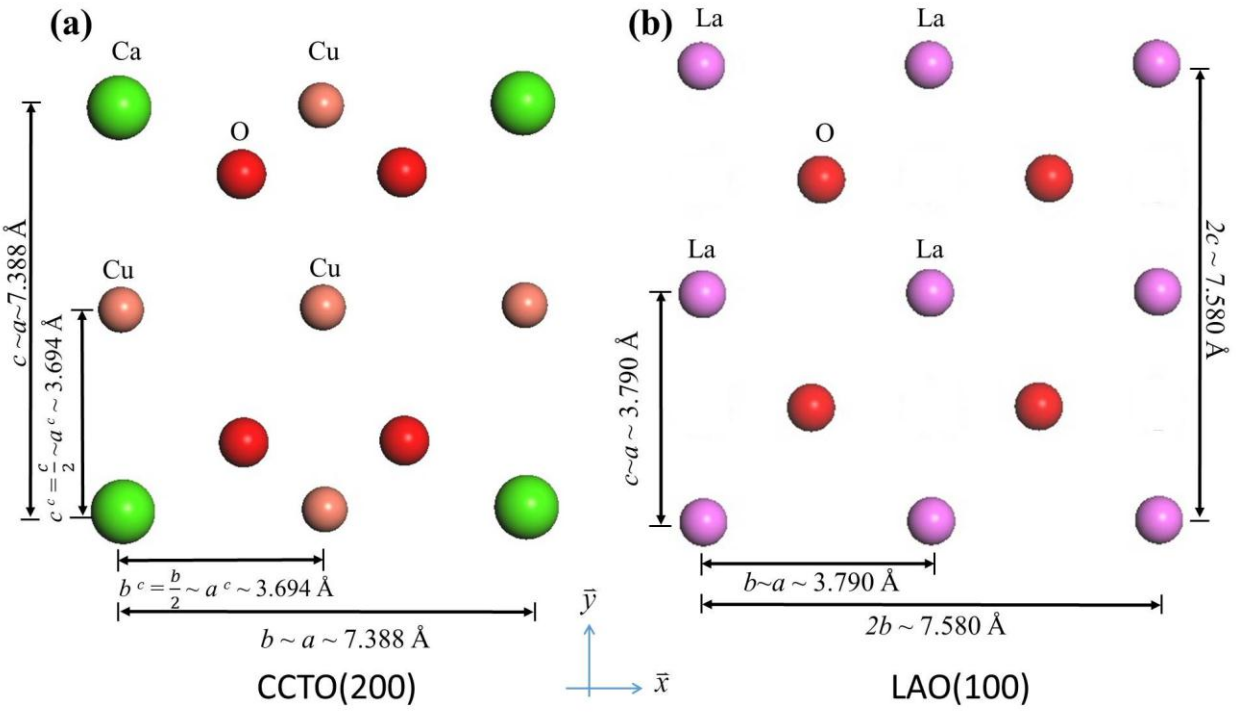

Fig 2. In-plane view of the crystal planes of (a) CCTO(200) and (b) LAO(100) substrate.

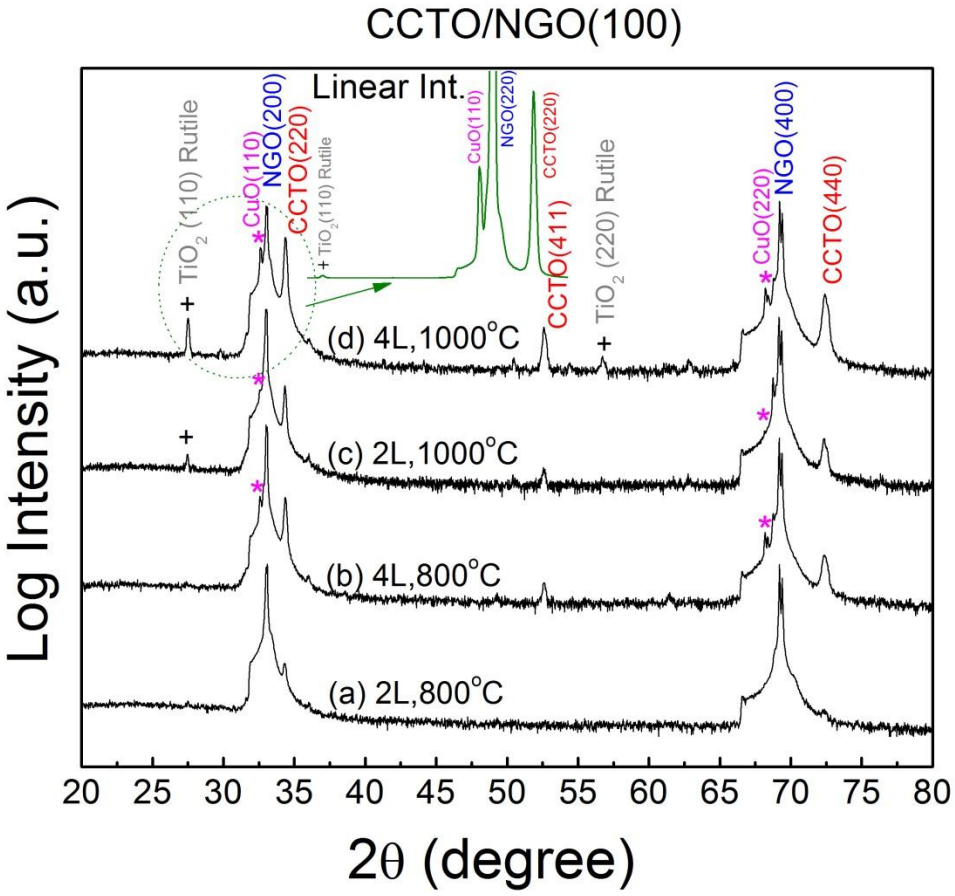

Fig. 3 θ-2θ X-ray diffraction scans of CCTO films deposited on NGO(100) substrates: (a) two-layered CCTO/NGO(100) annealed at 800 ºC, (b) four-layered CCTO/NGO(100) annealed at 1000 ºC, (c) two-layered CCTO/NGO(100) annealed at 1000 ºC, (d) four-layered CCTO/NGO(100) annealed at 1000 ºC. Note that the main plot is in log scale while the inset is the XRD pattern in linear intensity scale for film (d).

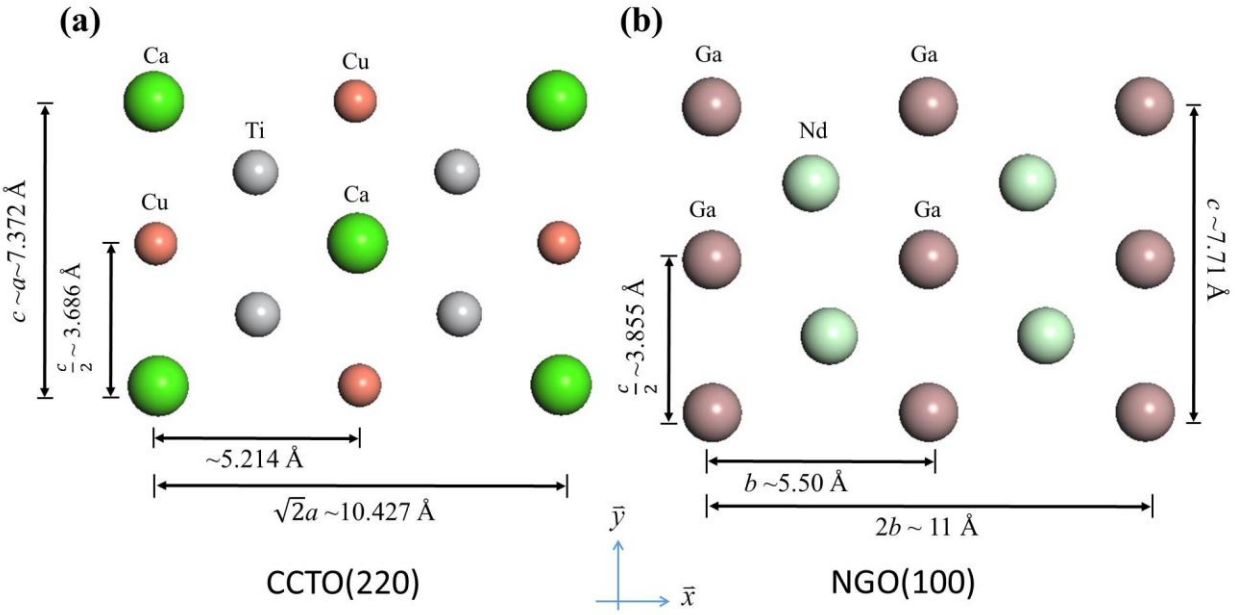

Fig 4. In-plane view of the crystal planes of (a) CCTO(220) and (b) NGO(100) substrate.

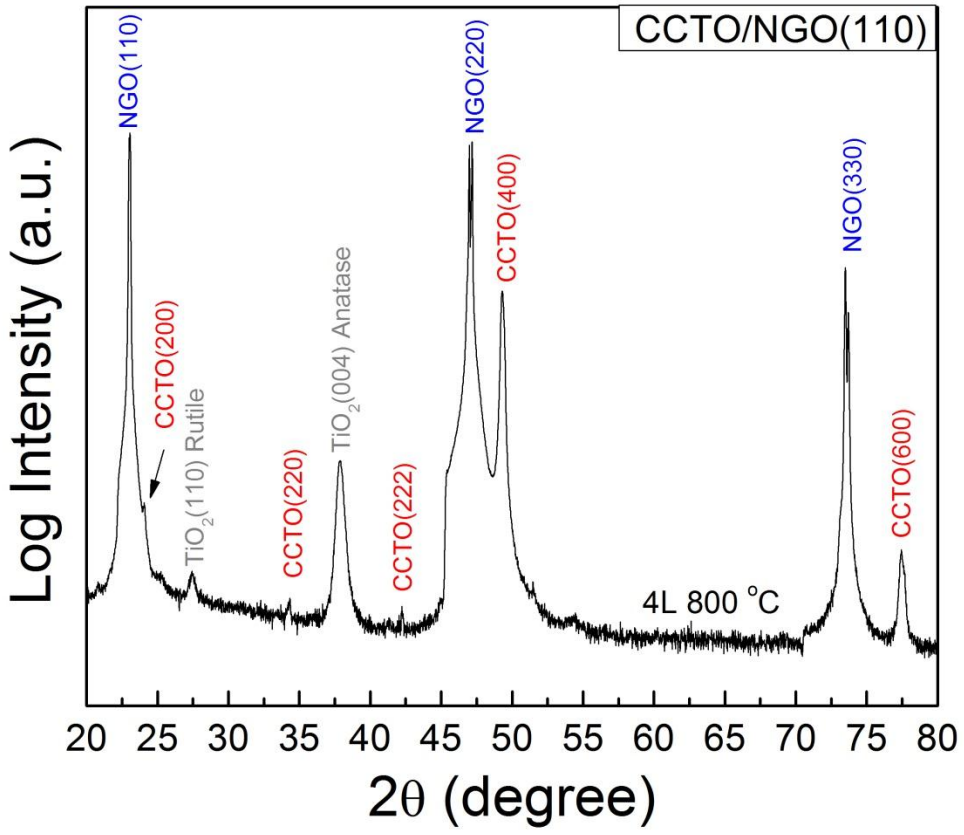

Fig. 5 θ-2θ X-ray diffraction scan of four-layered CCTO films deposited on NGO(110) substrate annealed at 800 °C. Note that the main XRD plot is in log scale.

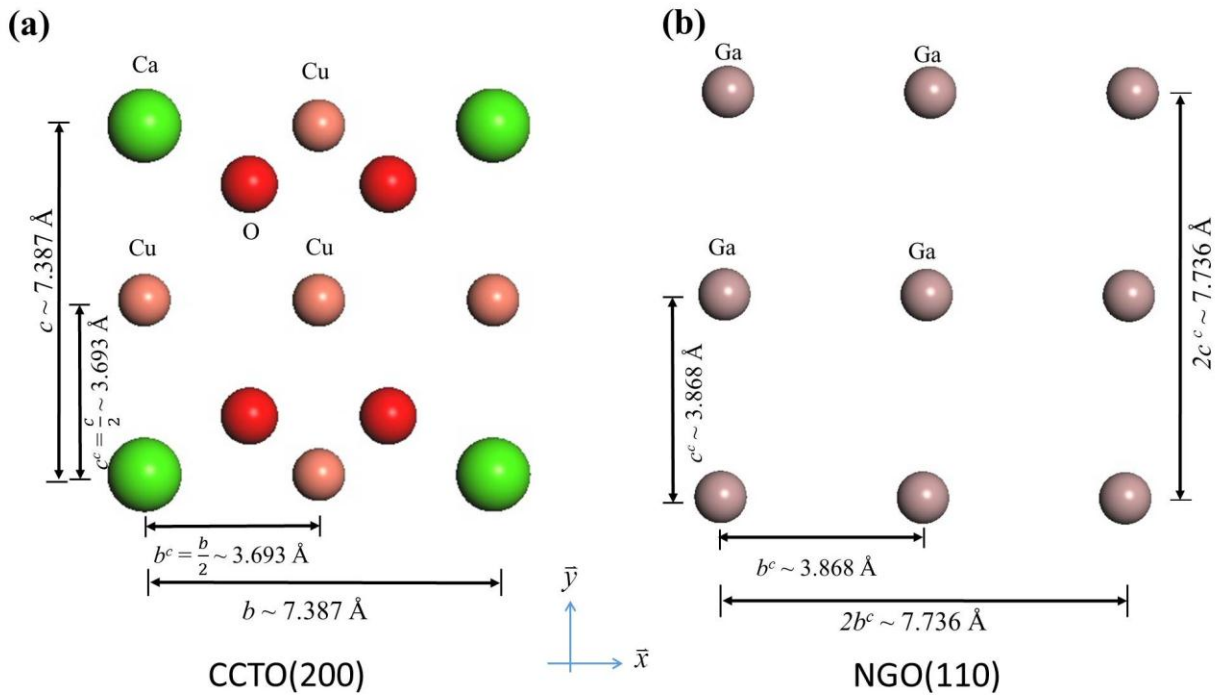

Fig 6. In-plane view of the crystal planes of (a) CCTO(200) and (b) NGO(110) substrate.

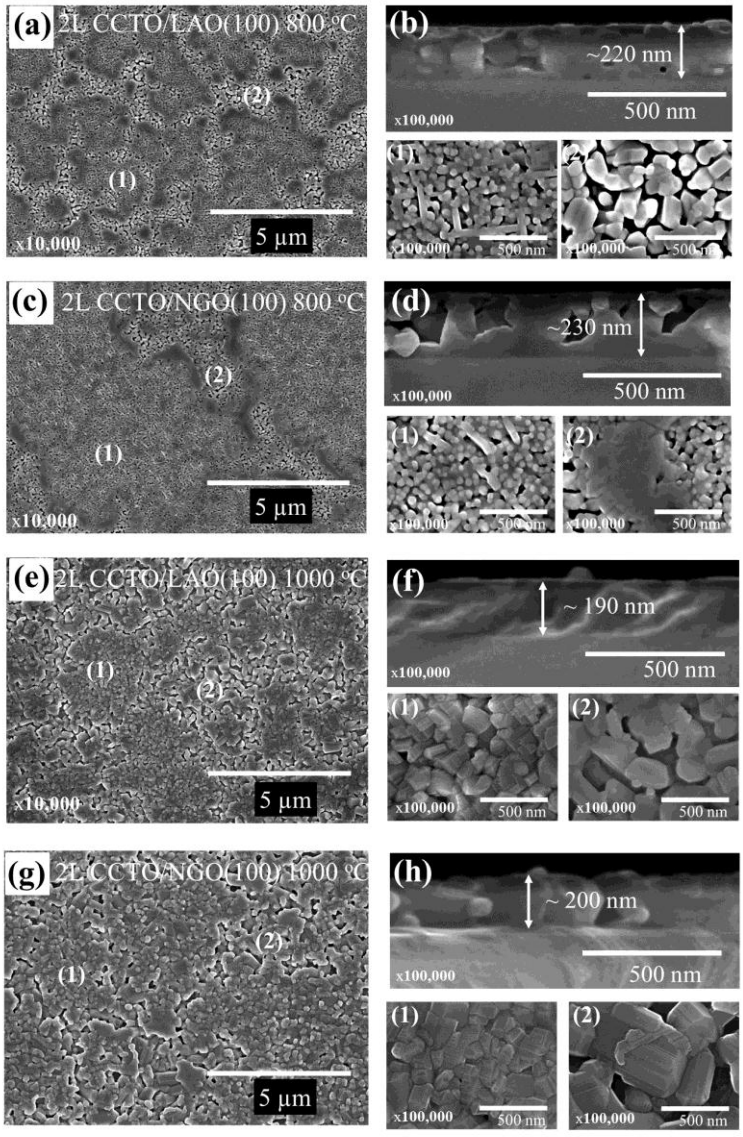

Fig.7 FE-SEM images of two-layered CCTO films (a) Plane view of CCTO/LAO(100) film annealed at 800 ºC and (b) the corresponding cross section and expanded views of areas (1) and (2), (c) Plane view of CCTO/NGO(100) film annealed at 800 ºC and (d) corresponding cross section and expanded views of areas (1) and (2), (e) Plane view of CCTO/LAO film annealed at 1000 ºC and (f) the corresponding cross section and expanded views of areas (1)

and (2), (g) Plane view of CCTO/NGO film annealed at 1000 ºC and (h) corresponding cross section and expanded views of areas (1) and (2).

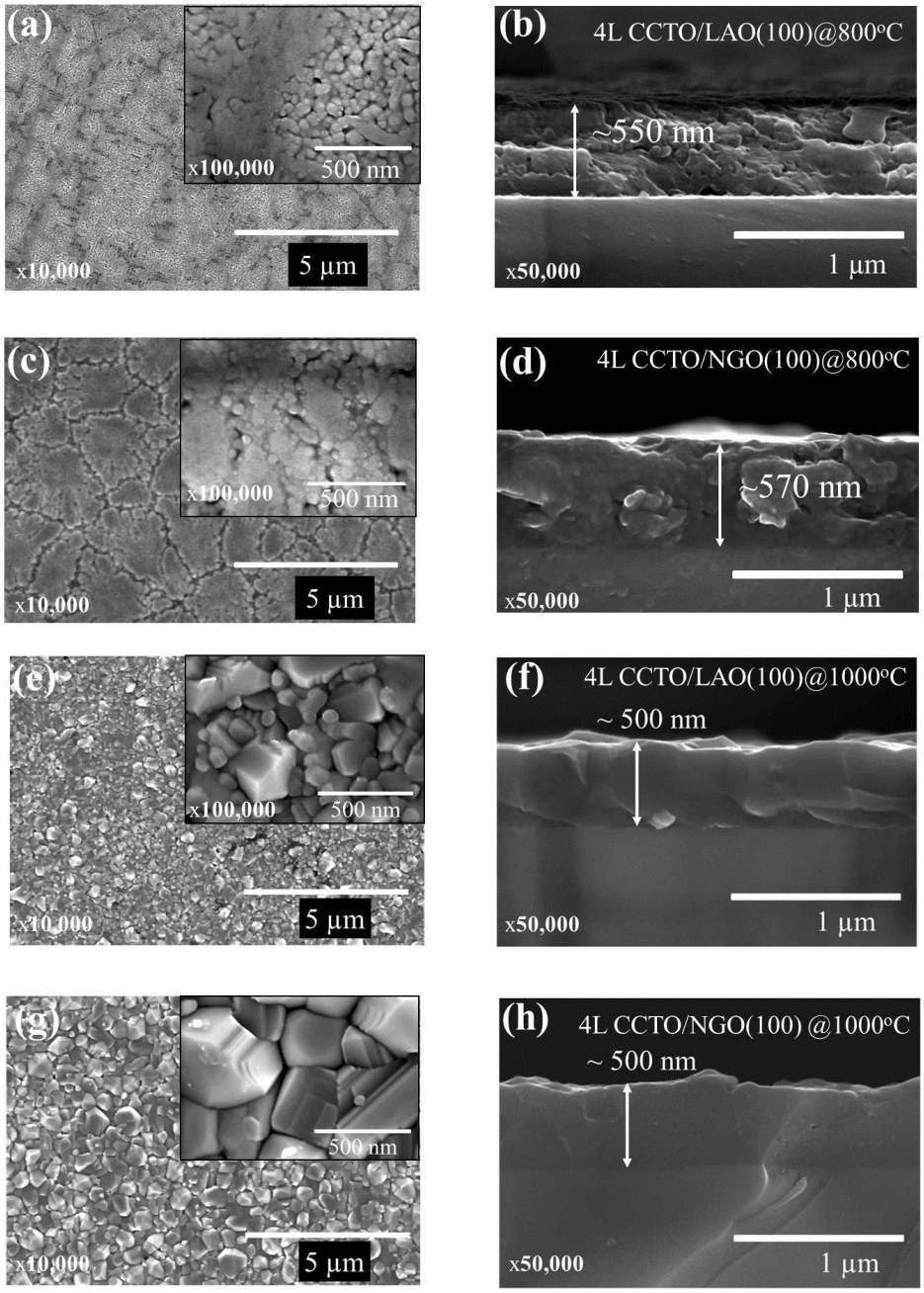

Fig.8 FE-SEM images showing the top view of four-layered CCTO films (left) and the corresponding cross sectional views (right); (a-b) CCTO/LAO(100) film annealed at 800 ºC,

(c-d) CCTO/NGO(100) film annealed at 800 ºC, (e-f) CCTO/LAO(100) film annealed at 1000 ºC, and (g-h) CCTO/NGO(100) film annealed at 1000 ºC.

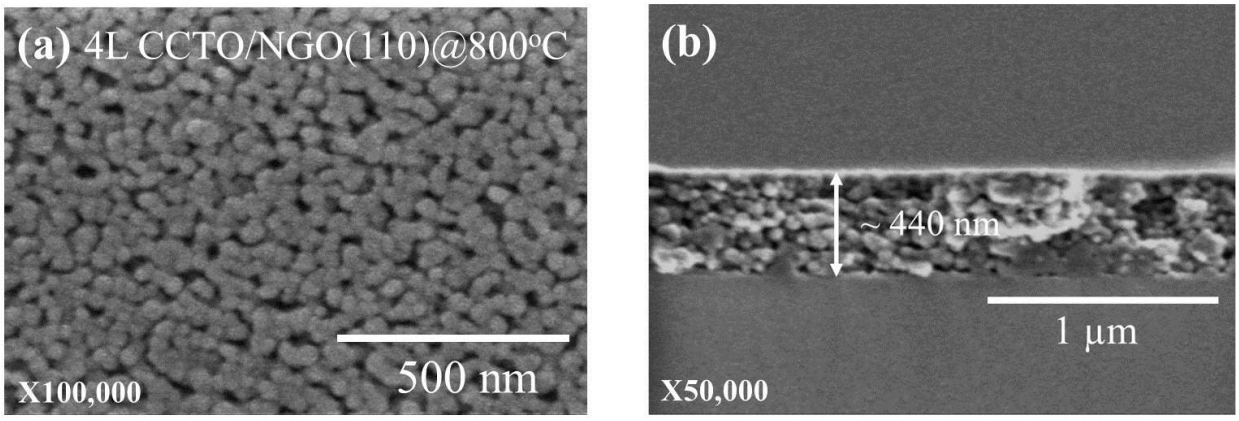

Fig.9 FE-SEM images of four-layered CCTO films on CCTO/NGO(110) substrate and annealed at 800 ºC; (a) top view of the film, and (b) corresponding cross sectional view.

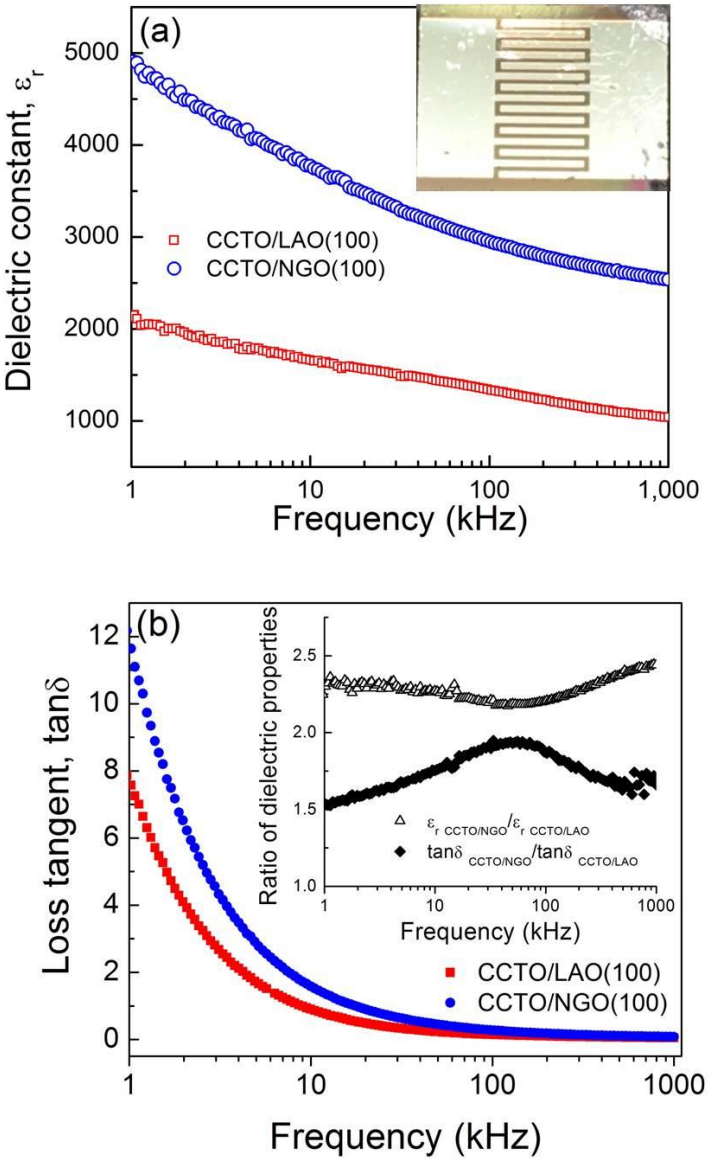

Fig. 10. (a) Top panel: dielectric constants of CCTO films on LAO(100) (open red squares) and NGO(100) (open blue circles) as a function of frequency. The inset in (a) shows an actual interdigitated capacitor used for the measurements. (b) Lower panel: corresponding loss tangent of CCTO films on LAO(100) (solid red squares) and NGO(100) (solid blue circles) The inset in (b) shows the ratios of the dielectric constant (triangles) and loss tangent (diamonds) for the film deposited on NGO(100) relative to that deposited on LAO(100).

Tables

Table 1: Comparison of the preferential orientation for CCTO films on LAO(100).

Growth Conditions		$\alpha_{(400)}$ Eq. (1)	$I_{(400)}^{film} / I_{(220)}^{film}$
Number of CCTO layers/substrate	Annealing Temp. (ºC)		
2L/LAO(100)	800	3.36	39.0
4L/LAO(100)		3.41	67.0
2L/LAO(100)	1000	3.04	7.3
4L/LAO(100)		3.19	11.8

Table 2: Comparison of the preferential orientation for CCTO films on NGO (100).

Growth Conditions		$I_{(220)}^{film} / I_{(411)}^{film}$
Number of CCTO layers/substrate	Annealing Temp. (ºC)	
2L/NGO(100)	800	no (411) peak
4L/NGO(100)		81.6
2L/NGO(100)	1000	73.2
4L/NGO(100)		106